Astrophysics of Dust
ASP Conference Series, Vol. 309, 2004
Adolf N. Witt, Geoffrey C. Clayton & Bruce T. Draine, eds.

Laboratory Studies of Carbonaceous Dust Analogs

Th. Henning

Max Planck Institute for Astronomy, Königstuhl 17, D-69117 Heidelberg, Germany

C. Jäger

Astrophysical Institute and University Observatory, Schillergässchen 2-3, D-07745 Jena, Germany

H. Mutschke

Astrophysical Institute and University Observatory, Schillergässchen 2-3, D-07745 Jena, Germany

Abstract.
This review summarizes progress in the laboratory investigation of carbonaceous dust analogs. After introducing the fundamental properties of solid carbon allotropes, production routes and means of characterization of carbonaceous grains are discussed. Spectroscopic features of carbonaceous dust analogs are of special interest in astronomy. They will be related to the structural properties of the material. We will also discuss the far-infrared properties of carbonaceous grains.

1. Introduction

Carbon is a very unique element of the periodic system. It is the first of the lighter elements in space that is exclusively formed by stellar nucleosynthesis. The 3 α process leads from ^{4}He to ^{12}C. This resonant formation process of ^{12}C, together with its non-resonant and therefore inefficient transformation into ^{16}O, forms the unique combination that is responsible for the presence of carbon in space. Carbon forms the basis of a rich organic chemistry in the solar system and the interstellar medium and finally for life on Earth and possibly on other planets. This feature is intimately linked to the special property of carbon atoms present in different hybridization states. Carbon is the element which most easily forms strongly bound clusters as known from soot production in flames. It has unique physical and chemical properties, especially in the transition zone between molecules and solids.

Carbonaceous grains are a dominant component of interstellar dust and form in large quantity in circumstellar envelopes around carbon stars. These grains provide the surface for the formation of molecular hydrogen and certainly other molecules in space. Very small carbon grains may be the dominant heating source for the diffuse interstellar medium via the photoelectric

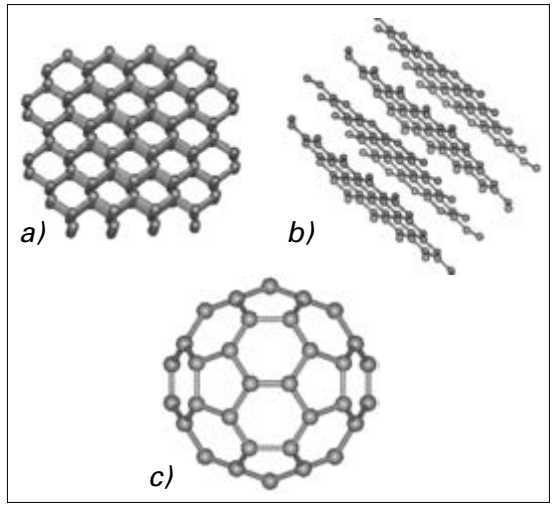

Figure 1. Crystalline carbon allotropes. a) Diamond, b) Graphite, and c) Fullerene.

effect. Furthermore, carbonaceous grains readily absorb and scatter stellar light from far-ultraviolet to near-infrared wavelengths and thermally radiate in the infrared and submillimetre wavelength domain. The latter process makes deeply dust-embedded high-mass protostars and carbon-rich AGB stars the brightest galactic infrared sources and allows the determination of circumstellar mass and temperature from an analysis of their submillimetre emission.

This review will summarize the basic properties of carbonaceous grains, their production in the laboratory and their analytical characterization. We will shortly discuss different formation routes of solid carbon. Finally, we will relate the structural properties of carbonaceous material to spectroscopic features, especially the electronic transitions at ultraviolet wavelengths relevant to the astronomical 217.5 nm feature. For other reviews, also including the atomic and molecular aspects of carbon in space, we refer to the papers by Henning & Salama (1998) and Ehrenfreund & Charnley (2000).

2. Solid Carbon Allotropes

The different types of carbon hybrid orbitals (sp, sp^2, sp^3) lead to different bond structures between carbon atoms. They are bound together through two different types of covalent bonds, the localized strong σ bond and the weaker π bond. The π bond can either be delocalized or form a localized double bond together with a σ bond. In acetylentic structures (sp^1), one σ and two π bonds are present between the carbon atoms, in aromatic or olefinic structures (sp^2)

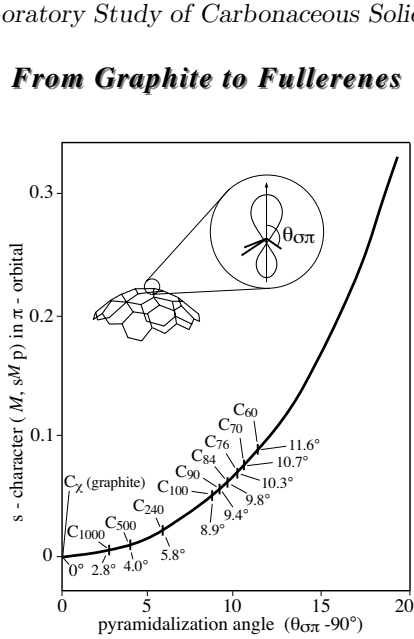

Figure 2. Pyramidalization angle from graphite to fullerenes. After Haddon (1993).

one σ and one π bond occur. Finally, saturated hydrocarbons (sp^3) contain only single σ bonds.

Pure solid carbon allotropes are graphite, diamond and the fullerene family (see Fig.1). In the case of graphite, carbon atoms are bonded to each other by both σ bonds and π bonds. The planar orientation of the sp^2 hybrid orbitals leads to a sheet-like crystal structure with anisotropic optical properties. The π orbitals are orthogonal to these planes. The π electrons are delocalized along the graphitic layers. This feature is responsible for a high conductivity along these layers. Carbon atoms in diamonds are covalently bonded to each other in a tetrahedral geometry via four σ bonds pointing to the corners of the tetrahedra. Diamond is characterized by a relatively large band gap of 5.5 eV. Fullerenes have a σ bond hybridization which falls between graphite and diamond. The σ bonds deviate from planarity and fullerenes show a curved structure. The smallest fullerene, C_{60}, has the highest number of 5-membered rings per usual benzene ring and is characterized by the largest pyramidalization angle $\theta_{\sigma\pi}$ (see Fig. 2). Carbon onions (Fig. 3) and carbon nanotubes are related structures (Iijima 1991, Ugarte 1992, Dresselhaus, Dresselhaus, & Eklund 1996). Bent graphene layers play an important role for the structure of carbon nano-particles (see, e.g., Harris et al. 1994, Rotundi et al. 1998, Jäger et al. 1999, Schnaiter et al. 1999, Wada et al. 1999). Sp-based crystalline carbyne has been proposed as another carbon allotrope (see Heimann, Evsyukov, & Kavan 1999 for a review book), but experimental evidence for this material is lacking, although stable carbyne-rich solids have been produced (Ravagnan et al. 2002).

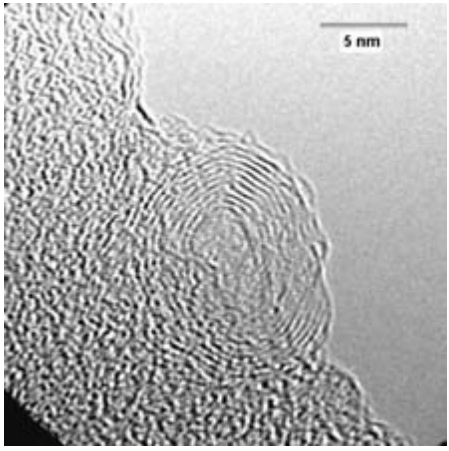

Figure 3. Onion particle detected in material from the Allende meteorite.

Although micron-sized graphitic spherules (and, with less confidence, nanodiamonds) of circumstellar orgin have been identified in meteorites (Ott 2003, Hoppe, this volume), it is now generally accepted that interstellar and circumstellar grains are not simply graphite, but should have a disordered structure with a some degree of hydrogenation.

A variety of disordered bulk materials have been produced in the laboratory or obtained from nature. In astrophysics a wide variety of designations for carbonaceous materials has been introduced which easily can lead to confusion. Therefore, we will shortly summarize what kind of bulk materials have been considered.

Much of our present knowledge on disordered bulk carbon comes from the study of hydrogenated amorphous carbon (a-C:H) films, prepared by different deposition techniques (Pouch & Alterovitz 1990, Robertson 1991). The most popular method to produce such films is the plasma deposition technique which involves radio frequency-, microwave- and laser-induced plasma decomposition of a hydrocarbon precursor gas. Hydrogenated amorphous carbons are usually classified according to their atomic C/H-ratio and/or the associated sp^2/sp^3 ratio. The optical properties of these thin films can be determined by both transmission and reflection spectroscopy. Depending on the hybridization mixture, the band gap ranges between 1.5 and 4.0 eV. The material is characterized by smaller clusters of distorted benzene, and 5- and 7-fold rings. Duley & Williams (1981) were the first who introduced this material as a possible analog for cosmic dust. They used the acronym "HAC" for this material, whereas Sakata et al. (1983) used the designation QCC for "quenched carbonaceous composite" (see

also Sakata et. 1994, Wada et al. 1999, and Goto et al. 2000 and references therein).

Like a-C:H, demineralized natural coal is a hydrogenated disordered carbon usually with a higher oxygen content compared with the hydrogenated carbon films. Coals are therefore classified according to their atomic ratios of heteroatoms (H, O) to carbon, and according to their level of graphitization. Natural coal was introduced into the astronomical literature by Papoular et al. (1989) who used it as a model first for the UIBs, and later for the interstellar extinction curve (Papoular et al. 1993). Here we would like to note that virtually all the carbon in interplanetary dust particles and meterorites has a kerogen-like structure, a term used for all different stages of coal (Cronin & Chang 1993, Cruikshank 1997). The meteoritic material consists of a three-dimensional network of polyaromatic units connected by short aliphatic bridges.

A further preparation technique for non-crystalline solid carbon is the pyrolyzation of cellulose at different temperatures (Jäger, Mutschke, & Henning 1998) which allows the production of material with various well-defined sp^2/sp^3 ratios. Heating of organic polymers can also lead to glassy carbon. Glassy carbon contains crumpled aromatic sheets or entangled ribbons and shows a metallic behaviour.

Detailed investigations of the optical properties of HAC films have been performed by Ogmen & Duley (1988), Duley (1994), and Scott, Duley, & Jahani (1997). Grishko & Duley (2002) studied infrared absorption and emission spectra of HAC prepared in the presence of oxygen, nitrogen, ammonia, and carbon monoxide.

The investigation of the interstellar 217.5 nm and the 3.4 μm features as well as the detection of emission from transiently heated particles brought carbonaceous nanoparticles in the centre of interest of laboratory investigations. Such particles can be produced by a large variety of techniques. A key feature of these techniques is the production of a supersaturated vapour either by the evaporation of bulk material (e.g. laser ablation, resistive heating of carbon rods, arc sputtering) or the decomposition of a precursor gas such as acetylene (e.g. laser or flame pyrolysis, radio frequency and plasma decomposition). The generated vapour is quenched in an inert gas (usually helium or argon) to achieve supersaturation and to trigger the condensation process. Carbon nano- and microparticles produced in hydrocarbon flames are known as soot or carbon black particles and can be produced under well-controlled conditions. The term carbon black is applied to carbonaceous products resulting from incomplete combustion (Donnet, Bansal, & Wang 1993). Examples of carbonaceous particles produced in the laboratory under different atmospheric conditions are shown in Fig.4.

Well-defined production conditions can also be obtained in the case of laser pyrolysis where a tailoring of the chemical composition and the size distribution of the produced particles is possible.

With the aim of finding an analog for interstellar grains, several authors investigated the absorption characteristics of nanosized disordered carbon grains with respect to the electronic band structure (Mennella et al. 1995a, Jäger et al. 1999), C-C and C-H vibrations (Herlin et al. 1998, Schnaiter et al. 1999), the particle clustering (Schnaiter et al. 1996, 1998), the stability against UV

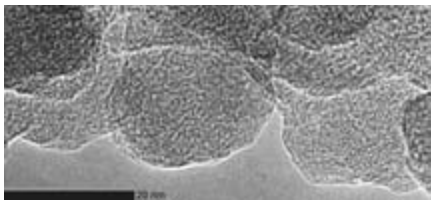

100 mbar He; curved graphene layers, concentric structures

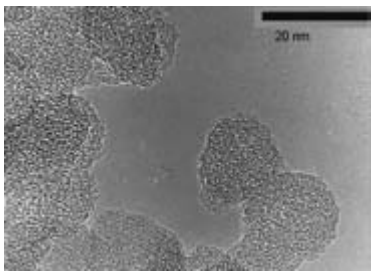

10 mbar He, amorphous structure

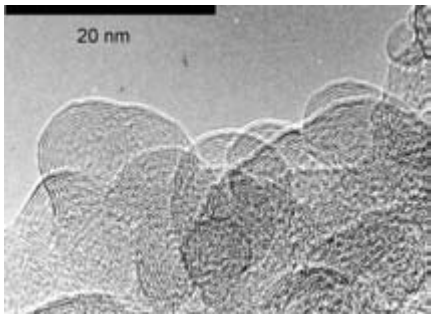

10% H_2, 90% He, onions

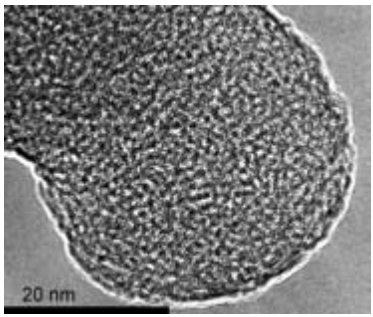

100 mbar Ar, graphitic soot, statistically distributed BSUs

Figure 4. Carbonaceous particles produced in the laboratory by evaporation of graphite electrodes under different atmospheric conditions.

and ion irradiation and atomic hydrogen exposure (Mennella et al. 1995b, 1996, 1997, 1999, 2002, 2003) as well as the microcrystallinity of the semi-conducting material (Koike et al. 1995, Michel et al. 1999, Rotundi et al. 1998).

Disordered carbon allotropes are usually characterized by the nearest neighbour bonding types (i.e. the sp^2/sp^3 ratio) and by the range, type, and order of microcrystallinity. In the case of extremely small particles, "size effects" may also play a role. An example is the limitation of the electron mean free path in conducting small grains and the metal-to-insulator transition (see Lonfat, Marsen, & Sattler 1999 for the change of gap energy with size). Here we should note that carbonaceous nanoparticles may have different structures from the bulk, and that bulk material may not exist as small spherical particles. Nanosized monocrystalline spherical graphite particles, often used in astronomical dust models, simply do not exist in the laboratory. Nanoparticles often contain onion-like bent structures. They can be divided into spherical and polyhedral carbon onions. These structures often contain a large number of defects. In addition, small particles are characterized by a large surface-to-mass ratio and many of the measured spectroscopic vibration features in the infrared are a surface phenomenon. Here we should note that non-planar onion-type carbonaceous nanostructures can play an important role in heterogeneous catalysis (e.g., Maksimova et al. 2000, 2001), a fact which is not yet realized in astronomy.

The structural properties on the various scales (see Fig.5) somehow define the electronic density of states, the band structure, and, therefore, the optical behaviour of the particles. In the case of small particles, there are additional size, shape, and clustering effects which influence the optical properties and sometimes strongly mask other structural effects (Rouleau, Henning, & Stognienko 1997, Markel & Shalaev 2001, Quinten et al. 2002). In the standard model of disordered carbonaceous solids, the electronic band structure near the band edges is determined by the size distribution of stacked plane graphene (sp^2) sheets (Robertson & O'Reilly 1987, Robertson 1991). These aromatic nanocrystalline stacks (basic structural units - BSUs) with sizes between 0.6 and 4 nm determine the transition between the localized and delocalized π states and, therefore, the size of the energy gap between the filled valence and the empty conduction bands. The localized π states of the smaller BSUs are found energetically in the band gap. Their size distribution defines the slope of the band edges. The optical properties are also defined by the orientation of the BSUs (Michel et al. 1999). An important modification of this picture is the presence of bent structures in a large range of nanoparticles. Fig.6 schematically summarizes the various models for soot particles

Fundamental parameters which have to be determined in order to reach a global understanding of the spectroscopic behaviour as a function of structural properties are the sp^2/sp^3 ratio and the related hydrogen content as well as the degree, size, and type of order on different scales. The obviously best, but also time-consuming, method to investigate the structural ordering, especially in the case of carbonaceous nanoparticles, is provided by high-resolution electron microscopy (HRTEM). The structural characterization of carbon black particles is closely linked with progress in electron microscopy (Heidenreich, Hess, & Ban 1968). X-ray diffraction and Raman spectroscopy are other techniques for characterizing the structural order. Electron energy loss spectroscopy (EELS),

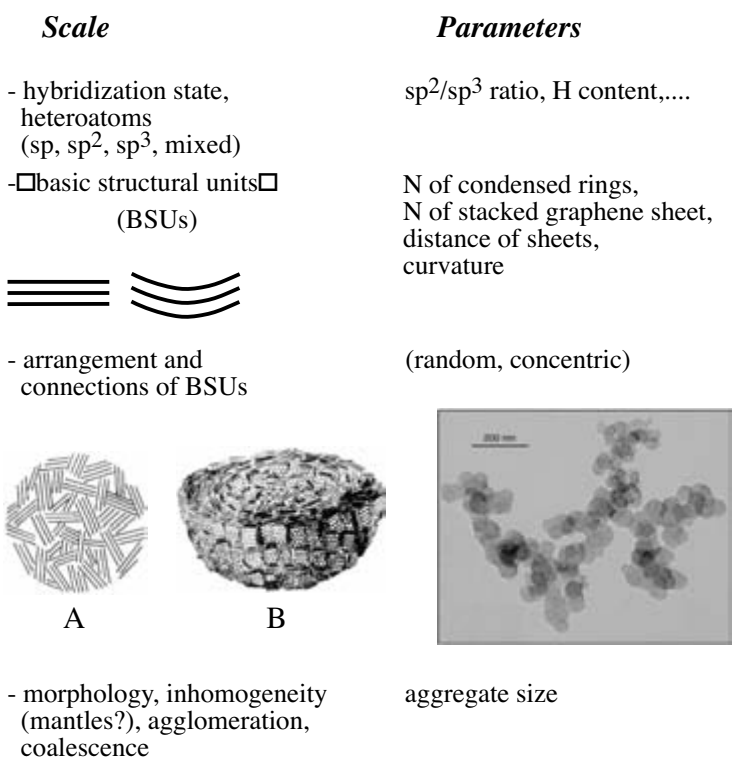

Figure 5. Amorphous carbon structures at different scales. The inserted figures A and B show two different types of the possible arrangements of BSUs in disordered carbon. The inserted figure in the right lower corner demonstrates the typical tendency of soot particles to form relatively large and fluffy aggregates composed of primary spherical particles.

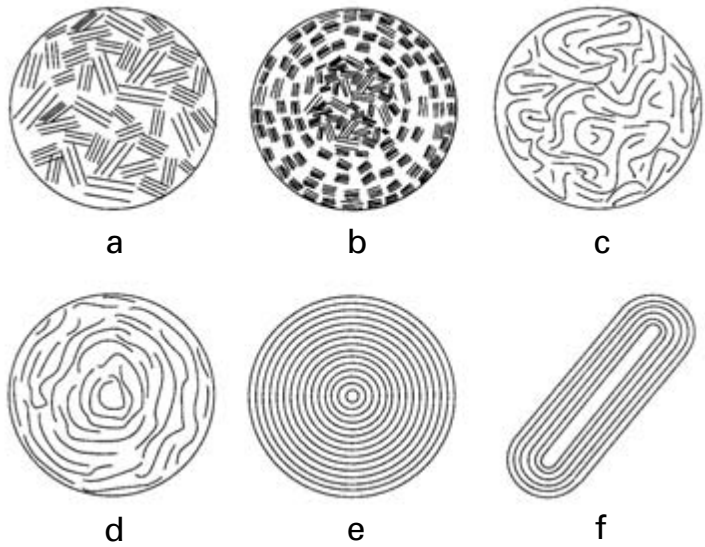

Figure 6. Models for graphitic structures in soot particles. (a) Plane BSUs - randomly distributed, (b) plane BSUs - concentrically distributed, (c) bent graphene layers - randomly distributed, (d) bent graphene layers - concentrically distributed, (e) onion particles, (f) nanotubes.

nuclear magnetic resonance (NMR), and optical spectroscopy from the ultraviolet to infrared wavelength range provide information about the sp^2/sp^3 ratio, the hydrogen content and the band structure. EELS can also map the elemental composition. Combustion analysis (CHONS) is an independent method for determining the elemental composition of the material. Table 1 summarizes the various analytic techniques along with their pros and cons.

Table 1. Structural characterization methods for carbonaceous materials

Method	Sensitivity	Pros	Cons
HRTEM	Global ordering	Direct insight into the carbon structure, degree, size, and type of ordering	Time-consuming search for representative structures
X-ray diffraction	Local ordering	Detailed coordination study	No simple interpretation
Raman spectr.	BSU sizes, degree of oder	BSU size determination	Only valid for plane BSUs
EELS	sp^2/sp^3 ratio, band structure, elemental composition, C allotropes	Direct comparison with HRTEM structures	No simple quantitative analysis
^{13}C NMR	sp^2/sp^3 ratio, detection of funct. groups	Absolute determination	Huge amount of sample required
UV/VIS spectr.	sp^2/sp^3 ratio, BSU size, gap energy, number of condensed rings	Fast, easy to apply in the visible and near UV	Influence of particle clustering, bent and plane structures cannot be distinguished, difficult in the FUV
IR spectr.	Hydrogen content, hydrogen sites, graphitisation degree	Fast and easy	Surface and matrix effects, also detects adsorbed material
CHONS	Elemental composition	Fast and easy	Large sample amounts, also physisorbed hydrogen detected

3. Formation and Stability of Carbonaceous Structures

Most of the information, concerning the formation of carbonaceous solids from the gas phase, comes from the combustion literature (e.g. Bansal & Donnet 1993). The proposed process follows a general scheme. It starts with the formation of the first two-dimensional nuclei which defines the transition from the

molecular system to a system of solid particles. It follows a strong surface growth of these nuclei by the addition of radicals on active surface sites and the formation of crystallites with sizes of the order of 1 nm. Further surface growth and coagulation leads to primary particles with diameters between 10 and 30 nm. Collisions of primary particles form large and fluffy aggregates which are stabilized by van der Waals forces. The sintering of these agreggates finally leads to coalescence between the particles.

The kinetic route from gas phase precursors such as acetylene and methane to the nuclei depends on the precursor gas, pressure, volume, and temperature of the reaction zone. This is a process difficult to characterize and still poorly understood. A detailed kinetic model for the formation of carbonaceous solids from acetylene, involving PAHs as intermediate steps, has been developed by Frenklach & Wang (1994). This model has been applied for the explanation of carbon dust formation in the envlopes of carbon-rich AGB stars (Frenklach & Feigelson 1989, Cherchneff, Barker, & Tielens 1993). A bottleneck in this synthesis process is the formation of the first aromatic ring. After the formation of the benzene ring, molecular growth continues by hydrogen abstraction and hydrocarbon addition. Thermodynamical factors restrict this process to a small temperature window with a value depending on the pressure (see Cau 2002 and references therein). This fact limits the size of the PAH nuclei to about 1 nm for typical conditions in circumstellar envelopes around carbon-rich AGB stars (Frenklach & Wang 1994). We should note that the process introduced so far is not the only formation process discussed in the literature, and alternative routes with/without PAHs as intermediate steps have been discussed: A major problem of the classical scheme for soot formation is the much too low production efficiency (Cau 2002). Coalescence of PAHs has been discussed as an important new process leading to a much higher rate of soot production (Hepp, Siegmann, & Sattler 1995, Kasper, Siegmann, & Sattler 1997). Whether this process is of astronomical relevance still has to be demonstrated. A schematic picture of soot formation developed by the Zürich group is shown in Fig.7. Based on mass spectroscopy, Homann (1998) has suggested the presence of so-called aromers as intermediate products and precursors for fullerene and soot particle formation in flames. Aromers should present a group of large and reactive fragments of 3-dimensional bent graphene layers similar to the saucer-shaped structures proposed by Kroto & Walton (1993).

We found in laser pyrolysis experiments (with acetylene and laser ablation of graphite under the conditions of a quenching gas atmosphere) that very small carbon grains with sizes between 1 and 4 nm form as original seeds. These seeds consist of strongly bent graphene layers (a disturbed cage-like structure), pointing to a formation mechanism via aromers or saucer-shaped structures (see Fig.8). These seeds agglomerate and build up larger primary particles with sizes up to 10 nm (Fig. 8a and 8b). Restructuring processes due to a long residence time of the agglomerated seed particles within the condensation zone can trigger the formation of more ordered and less bent graphene layers in the primary particles (see Fig.8c).

The formation route of carbonaceous particles from pure carbon vapours attracted a lot of recent attention because of the detection of fullerenes. It is a rapid process starting with linear C_3 and C_2 molecules, finally leading to

cyclic rings and structures with curved graphene layers and three-dimensional fullerenes and nanotubes (e.g. Seifert, Becker, & Dietze 1988, von Helden et al. 1991, Smalley 1992, Curl 1993, Kroto & Walton 1993). This formation process is certainly of less interest in astrophysics, but may play a role in carbon dust formation in the envelopes of the carbon-rich and hydrogen-poor R Coronae Borealis stars. However, elements of this process such as the isomerization of polycylic polyyne rings to bent graphene layers and fullerenes may also be present in certain hydrocarbon environments.

There is a wide range of transformation processes among different carbonaceous solids, especially if the material is heated, exposed to atomic hydrogen or irradiated by UV photons and ions (e.g. Mennella et al. 1996, 1997, 1999, 2002, 2003, Goto et al. 2000). Exposure with hydrogen can activate the 3.4 μm band, whereas UV and ion irradiation leads to the destruction of C–H bonds. We will not discuss these processes, but refer to the papers by Mennella et al. and his contribution in this volume. However, we want to discuss a few additional aspects of the transformation process of nanoparticles.

Carbon onions can be produced by a number of techniques. It is interesting to note that diamond nanoparticles can be transformed into carbon onions by thermal annealing (Kuznetsov et al. 1994, Obraztsova et al. 1998, Tomita et al. 1999, Braatz et al. 1999), starting from the surface and continuing to the centre. The transformation temperature is around 600 °C for meteoritic nanodiamonds (Braatz et al. 1999). Under ultra-high vacuum conditions or in a pure hydrogen atmosphere, the transformation of diamond into graphite occurs at about 1500 °C (Evans 1992). The graphitisation process can be catalysed by traces of oxygen in the atmosphere. The low transformation temperature for meteoritic diamonds can be caused by abstraction of oxygen from the strongly oxidized surface of the meteoritic nanodiamonds during annealing.

Carbon onions can also be produced from amorphous carbon either by electron irradiation (Ugarte 1992, Banhart 1994, Zwanger, Banhart, & Seeger 1996) or ion irradiation (Weselowski et al. 1997). Well ordered onions are reported to be stable only under irradiation (Banhart 1999). High-temperature irradiation leads to the formation of very well-developed carbon onions with spacings between the shells lower than those between layers of graphite. A decrease from 0.28 nm close to the surface up to 0.22 nm in the centre of the onions is typical of those onions. Continued particle irradiation of these compressed carbon onions can trigger diamond nucleation in the centre (Banhardt & Ajayan 1996, Banhart 1997, Wesolowski et al. 1997). It turns out that ion irradiation with 3 MeV Ne^+ ions is much more effective than electron irradiation. The diamond nucleation is probably caused by a combination of high pressure in the centre of the carbon onions and the knock-on process by particle irradiation. The process can lead to a complete conversion of the onion into cubic diamond.

These experimental facts are especially interesting because both nanodiamonds and onions are found in primitive meteorites. It may suggest a link between these structures.

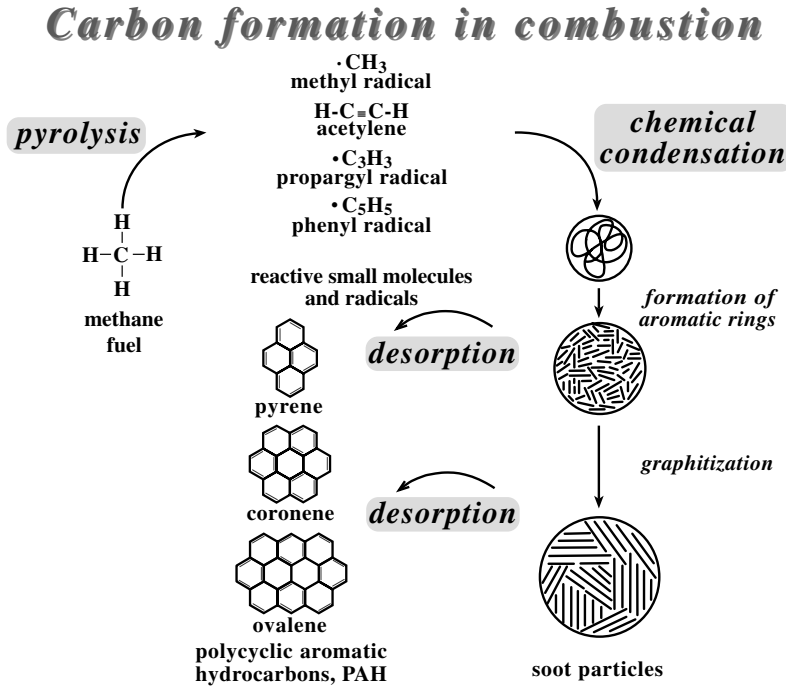

Figure 7. Schematic picture of carbon formation by combustion including chemical condensation from the vapour (reactive small molecules and radicals). Primary particles may consist of chain-like aggregates interconnected by flexible hydrocarbon chains. During heating in the flame the chain-like aliphatic structures are converted into aromatic rings. PAHs may detach from the surface of the particles. The heating process leads to larger BSUs and the particles become more graphitic. After ETH Zürich, Physics Department.

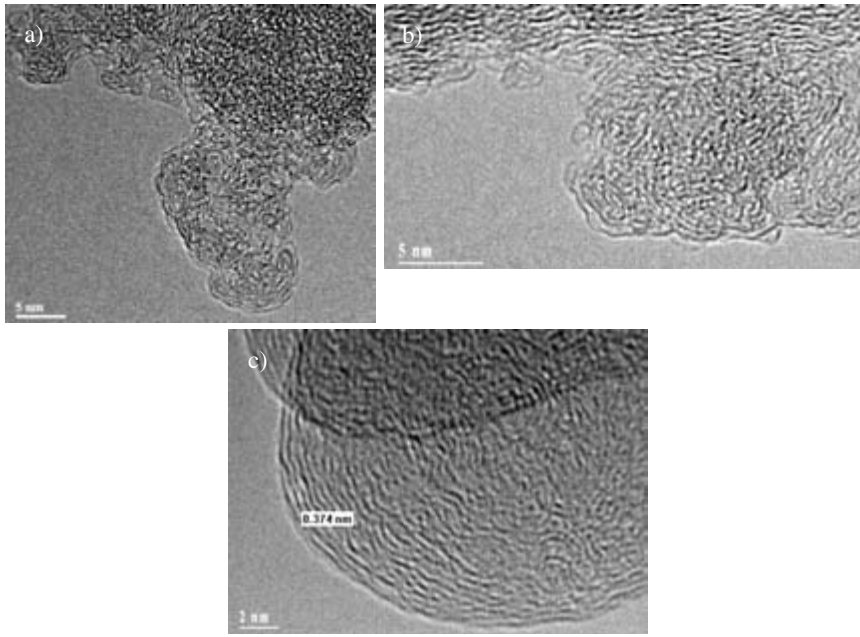

Figure 8. HRTEM images of soot particles formed by laser ablation of graphite and in laser pyrolysis experiments. Very small particles (1-4 nm) represent the original condensation seeds, which can form larger particles (up to 10 nm) by agglomeration and coalescence. The larger particles are still showing the original seeds. a) Particle produced by laser pyrolysis of acetylene. b) Particle produced by laser ablation of graphite. c) Restructured particle (laser pyrolysis) produced by long residence time in the condensation zone.

4. Astronomical Features and Laboratory Spectroscopy

Physical models for cosmic dust rely on optical properties measured in the laboratory. There are two different approaches for characterizing extinction and scattering properties of small particles (see, e.g., Henning & Mutschke 2000 for a review). The classical method is the determination of the optical constants of bulk material and the use of these data as input for small-particle scattering calculations. These are Mie calculations in the simplest case of small spherical particles or more complicated methods in the case of non-spherical, inhomogeneous, or agglomerated particles. This approach has been widely used in astronomy. An example is the assignment of the 217.5 nm bump to small nano-sized graphite particles with the optical constants coming from bulk graphite (Stecher & Donn 1965, Draine 1989). We have already stressed that the chemical and physical structure of small particles can differ significantly from the solid-state structure of the bulk phase (Henning 1998). This is especially true for carbonaceous grains with their structural manifold on all length scales. The structural diversity between the crystalline bulk phase and the nanoscale carbon grains is a strong argument against the hypothesis that graphite is the carrier of the 217.5 nm feature. The other approach for determining optical properties of dust analogs is based on transmission measurements on small-particle systems. In this case, the importance of size, shape and clustering effects has to be critically evaluated as long as no measurements on isolated particles with a narrow size and shape distribution are performed.

The optical behaviour of carbonaceous solids at ultraviolet wavelengths is determined by electronic transitions. The transition from the binding to the non-binding σ states is located between 80 and 100 nm wavelength. In the case of material which contains sp^2 hybridized carbon, a second transition occurs between 180 and 260 nm, caused by the electronic transition from the binding to the non-binding π states. The presence of a surface plasmon vibration has been discussed for spherical graphitic nanoparticles. A surface plasmon excitation occurs for ϵ = -2 $\epsilon_{\rm m}$, where ϵ is the dielectric function of the material and $\epsilon_{\rm m}$ the value of the surrounding medium. This resonance would be sensitive to shape and size effects, but this problem could be partly eliminated if the particles were nano-sized onions from the very beginning. The infrared spectrum of hydrocarbons is dominated by different vibrational modes which are again sensitive to the sp^2/sp^3 ratio (see, e.g., Henning & Schnaiter 1998). The far-infrared continuum behaviour is dominated by interactions with free, more or less delocalized charges.

Spectroscopic evidence for carbonaceous dust comes from the 217.5 mm feature in the diffuse interstellar medium (ISM) (Stecher 1965, Fitzpatrick & Massa 1986), a 240-260 nm exctinction peak in some carbon-rich stars (Hecht et al. 1984, Buss, Snow & Lamers 1989), the 3.4 μm "aliphatic" absorption feature in the diffuse ISM and absorption/emission features around this wavelength in post-AGB stars (Willner et al. 1979, Chiar et al. 1998, Pendleton & Allamandola, 2002, Goto et al. 2003), related 6.85 and 7.25 μm features in the spectrum of the galactic centre source Sgr A* (Chiar et al. 2000), a broad absorption band at about 3.3 μm in galactic centre sources (Chiar et al. 2002), posssibly caused by aromatic hydrocarbons, 3.43 and 3.53 μm emission features in the spectra of Herbig Ae/Be stars and possibly a post-AGB star attributed to nanodiamonds

(Guillois, Ledoux, & Reynaud 1999, van Kerckhoven, Tielens & Waelkens 2002, Sheu et al. 2002), and features at 3.47 μm (Allamandola et al. 1992), 4.62 and 6.0 μm in the spectra of dust-embedded young stellar objects (Gibb & Whittet 2002). In addition, one should not forget the contribution of carbonaceous particles to the general continuous extinction and infrared emission. The recent detection of the 217.5 nm feature in a lens galaxy at z=0.83 is a remarkable achievement (see Motta et al. 2002 also for a discussion of the presence of this feature in other galaxies). The extended red emission observed in a variety of objects was always associated with some carbon-containing solid. However, this was recently questioned by Witt, Gordon & Furton (1998) and Ledoux et al. (2001).

4.1. The 217.5 nm feature

The 217.5 nm feature is the only feature in the extinction curve observed at ultraviolet wavelengths (Clayton et al. 2003). Systematic investigations of the ultraviolet extinction along different lines of sight have shown that the bump position is remarkably stable, whereas the strength and width of the feature varies with line of sight (broader and weaker in denser regions) (Fitzpatrick & Massa 1986, Fitzpatrick 1999). It has been demonstrated both theoretically and experimentally that the broadening and weakening of the UV bump without an appreciable band shift can be explained by an agglomeration of small carbonaceous grains to small aggregates (Rouleau et al. 1997, Schnaiter et al. 1998). We should note that the bump parameters are not correlated with the far-UV rise of the extinction curve (Fitzpatrick & Massa 1988), pointing to different carriers or mechanisms for the two phenomena. The UV bump is certainly exclusively an absorption feature.

The two main problems in explaining the 217.5 nm feature on the basis of laboratory absorption spectroscopy are the narrow bandwidth and the nearly stable peak position of the feature. In addition, one should understand which materials have the feature at the right position.

Scattering calculations for spherical nano-particles with the optical constants of bulk graphite give a satisfactory representation of the observed mean interstellar extinction profile (Draine 1989). However, there are some serious problems with the graphite hypothesis: (i) Graphite is an anisotropic bulk material and is unlikely to be present in the form of monocrystalline spherical graphite nanoparticles, (ii) carbonaceous particles show a large diversity of structures, (iii) a fine-tuning of the bulk optical constants is required to fit the feature, (iv) the peak position of the plasmon resonance is quite sensitive to grain size, shape, and coatings inconsistent with the observations, and (v) formation routes in space are not expected to lead to graphite. Although there are some attempts to explain the feature by a mixture of large PAHs (Joblin, Léger, & Martin 1992, Beegle et al. 1997), solid carbonaceous nanoparticles are now the best candidate for the feature.

The position of the UV bump is determined by the electronic structure of the solid. Jäger et al. (1999) demonstrated that an increasing sp^2/sp^3 ratio can move the band from 220 nm to 270 nm, excluding very graphitic material as the band carrier. Here we should stress again that smaller particles often contain bent structures and, therefore, mixed hybridization states. Despite a higher

degree of ordering, they are less graphitic than larger particles. This behaviour is caused by an increase of the s-character of the π bond with bending (see Figs. 2 and 3). This implies that plane/bent systems with different states of order can lead to similar band positions. A higher hydrogen content in the experiments led to smaller particles (average size about 10 nm) and a shift of the feature to shorter wavelengths. It is remarkable to note that a saturation effect could be observed in the nanoparticle experiments by Schnaiter et al. (1998). When a certain small amount of hydrogen was present in the reaction chamber, the band position shifted to about 214 nm (matrix corrected) and remained nearly constant until a very large amount of hydrogen was offered.

In the case of larger primary soot particles with plane graphitic BSUs, we can observe a correlation between band gap energy, number of condensed rings and the position of the UV band. With larger BSUs the band gap decreases and the bump moves to longer wavelengths (Robertson & O'Reilly 1987, Jäger et al. 1999). In contrast to this model and the discussion by Mennella et al. (1995b), the experiments by Schnaiter et al. (1998) and Jäger et al. (1999) suggest that the presence of hydrogen does not really lead to smaller BSUs, but that hydrogen catalytically causes the production of bent and onion-type structures. A possible explanation for this formation route is the increase of temperature through the reactivity of hydrogen which would maximize the implementation of 5-fold rings and would favour the production of bent structures. This leads to the interesting question of whether a particulary stable onion-type carbon configuration exists in space that could explain the stability of the band position. In this context it is important to note that onion-type structures are favoured over planar BSUs and are energetically stable (Tománek, Zhong, & Krastev 1993).

Onions have already been proposed by de Heer & Ugarte (1993, see also Wright 1988) as the carrier of the UV bump, shortly after their detection. However, they had to shift the observed feature heavily to the blue in order to fit the interstellar feature, which was explained by the water environment of the experiment. Lucas, Henrard, & Lambin (1994) did theoretical calculations for carbon onions with a core material and found that a representation of the UV bump is possible, although the peak position and width depends on the core-to-graphitic shell size ratio. This already points to a weakness of the hypothesis which is similar to the situation for graphite. We expect to have a variety of carbon onion sizes and structures which would result in different spectra. Tomita, Fujii, & Hayashi (2002, see also for a good overview of the field) investigated the optical behaviour of both spherical and polyhedral onions and found a broad extinction peak for spherical onions and two peaks for polyhedral particles. Chhowalla et al. (2003) obtained ultraviolet-visible absorption spectra of high-purity and well-separated carbon onions which match relatively well the observed interstellar features. How such pure onions can be produced in astrophysical environments and how reproducable the results are remain open questions. In general, we would expect strong bending of graphene layers for smaller particles with the UV bump at short wavelengths. Larger particles would show much less bending, especially in the outer graphene layers. The more grahite-like optical behaviour would lead to a shift of the feature to longer wavelengths.

A related idea to the previous discussion of a stable system is the proposal that the evolution of the carbonaceous material in a cycle of hydrogenation

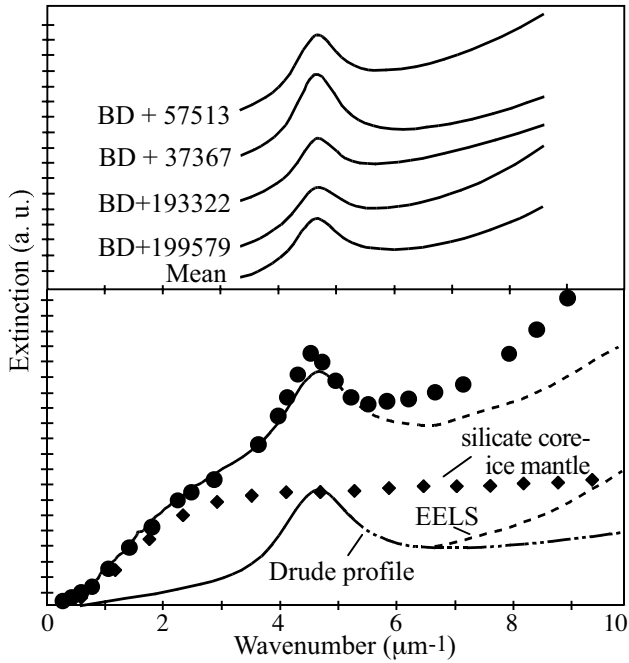

Figure 9. Upper part: Examples of interstellar extinction features; Lower part: The mean interstellar extinction curve (dots) can be reproduced by a sum (solid line) of the extinction from silicate core-mantle grains (diamonds, see Li & Greenberg 1997) and the absorption by matrix-isolated nanoparticles (lower solid curve, see Schnaiter et al. 1998). The dashed-dotted curve is an extrapolation of the Drude profile fitted to the measurements. The thin dashed line indicates the contribution from the σ-σ^* transition, based on the dielectric function obtained from EELS.

and dehydrogenation is responsible for the observed spectroscopic features (see Mennella, this volume).

The puzzle of the narrow width of the observed feature compared with laboratory data and the lack of correlation between bump position and width were finally solved by the experiments of Schnaiter et al. (1998) (see Fig. 9). They were able to get spectra of nano-sized isolated hydrocarbon grains at low temperatures. In the experiments a clear correlation was found between the width of the π-π^* transition and the degree of clustering. Despite these changes, the UV bump remained at the same position. Such a behaviour was predicted by scattering calculations (Rouleau, Henning, & Stognienko 1997) and had been proposed as an explanation of the observed variations in the 217.5 nm feature widths. In the case of isolated nanoparticles (sizes of about 5 nm), the peak of the UV bump profile is found at 214 nm, very close to the interstellar peak

position, and with the right profile width. The particles can be best described as nanoparticles composed of concentrically ordered bent graphene layers.

4.2. The "aliphatic" 3.4 μm feature and related features

One of the primary infrared features pointing to carbonaceous dust in the diffuse interstellar medium is the 3.4 μm absorption feature, produced by an aliphatic hydrocarbon material. It is remarkable that this feature is not observed in carbon-rich AGB stars, but has been detected in some post-AGB stars. Experiments demonstrated that the profile of material produced from acetylene by laser pyrolysis does not fit the astronomical band profile (Schnaiter et al. 1999). Carbon grain formation from acetylene should be the primary grain formation route in carbon-rich AGB stars. The experiments support the view that the carrier material is not formed during the AGB phase. In contrast to this, Schnaiter et al. (1999) found that the same material fitting the UV bump also has a band profile which provides an excellent fit to the observed 3.4 μm profile. They suggested that the feature is activated by hydrogen exposure, an idea which was followed-up by Mennella et al. (1999). This could also be a possibility for explaining the origin and difference of the feature in the diffuse interstellar medium and the dense molecular clouds (see Mennella this volume). An interesting observational fact comes from AO-assisted spectroscopy, showing that the intensity of the aliphatic hydrocarbon emission relative to the aromatic hydrocarbon emission decreases with distance from the star (Goto et al. 2003). Pendleton & Allamandola (2002) performed a very comprehensive evaluation of different laboratory analogs in the 2.5 to 10 μm spectral range. We refer the reader to this excellent review for more detailed information (see also the contribution by Pendleton in this volume). Pendleton & Allamandola concluded that the carbonaceous material responsible for the infrared features contains little oxygen and nitrogen. The carrier is best represented by plasma-processed hydrocarbon materials with aliphatic character and some aromatic component, but not by a UV or ion irradiated ice mixture (see also Shenoy et al. 2003).

4.3. The 3.43 and 3.53 μm "diamond" features

Nanodiamonds attracted a lot of attention because they are present in chondritic meteorites and could have a stardust origin (Lewis et al. 1987, Ott 2001, 2003). However, the isotope anomaly criterion fails in the case of nanodiamonds because of their small sizes (a few nm) which makes the isotopic analysis of individual grains impossible. Therefore, we do not know which fraction of the meteoritic nanodiamonds have a stardust origin. Meteoritic nanodiamonds may not have a stardust origin at all and the isotopically enriched gases, normally associated with the nanodiamonds, could be carried by contaminants. In addition, it turned out to be extremely difficult to obtain an unbiased infrared spectrum of nanodiamonds isolated from meteorites (Braatz et al. 2000, Mutschke et al. 1995) in order to compare such data with astronomical observations.

On the basis of experimental data from Chang et al. (1995), Guillois, Ledoux, & Reynaud (1999) quite convincingly identified features observed at 3.43 and 3.53 μm in the spectra of a number of Herbig Ae/Be stars with CH stretch bands of H-terminated diamond. There is also evidence that these features are present in the spectrum of the post-AGB star HR 4049 (Geballe et al.

1989, van Kerckhoven et al. 2002). The bands are a typical surface phenomenon. They broaden and redshift with increasing temperature (Chin et al. 1995, Lin et al. 1996). In addition, the 3.53 μm feature is only present if the diamond crystallites are larger than 25 nm (Sheu et al. 2002). This is a size range much larger than in the case of meteoritic nanodiamonds.

There is much evidence that nanodiamonds in the circumstellar environment of Herbig Ae/Be stars are not stardust, but in-situ products of a CVD-like (chemical vapor deposition) process (van Kerckhoven et al. 2002, Sheu et al. 2002; see also Braatz et al. 2000 and Duley & Grishko 2001).

4.4. Far-infrared Optical Properties

The far-infrared and submillimetre optical properties of carbonaceous solids are an important factor in determining the temperature of the dust grains. In addition, they are widely used to derive dust masses from continuum observations of optically thin configurations. The far-infrared optical properties of carbonaceous solids are a complicated interplay between the hybridization state and band gap of the material and the agglomeration and coalescence of the primary particles. This is especially true for conducting graphitic grains, where percolation (formation of extended conducting paths) can strongly enhance the absorption per unit volume (Stognienko, Henning, & Ossenkopf 1995).

Laboratory far-infrared measurements on amorphous carbon particles dispersed in polyethylene pellets usually reveal a power-law wavelength dependence of the absorption coefficient with the negative exponent β having values between 0.6 and 1.2 (e.g., Mennella, Colangeli & Bussoletti 1995). The mass absorption coefficient at a wavelength of 1 mm is of the order of 100 $\mathrm{cm^2 g^{-1}}$, which is much higher than for silicates. According to Koike et al. (1995), the exact β value is directly correlated to the size of the graphitic nanocrystallites (BSUs) building up the material, with larger BSUs leading to higher β values. The far-infrared spectrum of aerosol soot particles (Bruce et al. 1991) shows a similar behaviour.

Calculations of the absorption coefficient for isolated spherical particles generally fail to reproduce these values, but give absolute β values of roughly 1.2 to 2.3, i.e. a factor of two higher (e.g., Jäger et al. 1998) and an absorption coefficient at λ=1 mm which is two orders of magnitude too low compared with the pellet measurements. This discrepancy is at least partly related to the agglomeration and coalescence of the particles measured in the polyethylene pellets (Rouleau & Martin 1991). The influence of coagulation of spherical particles on their scattering and extinction properties nowadays can be modelled numerically by applying generalized Mie codes and other approaches (for a comparison see Michel et al. 1996 , Markel, Shalaev, & George 2001, Andersen et al. 2002). Such calculations for open and compact aggregate structures show that agglomeration of spherical amorphous carbon particles can enhance the far-infrared absorption by about one order of magnitude (Quinten et al. 2002). This effect depends on the conductivity of the material. However, the effect of coalescence can be much stronger, as can be demonstrated either by effective medium considerations (Stognienko, Henning, & Ossenkopf 1995) or by taking elongated particles as an analog (Quinten et al. 2002).

So far, the far-infrared absorption of coalesced particles cannot be modeled in a realistic way. However, it is remarkable that a mixture of more or less elon-

gated particles (continuous distribution of ellipsoids - CDE) provides a quite good match to the experimentally measured wavelength dependence of the absorption coefficient (Mennella et al. 1995). Therefore, this model has been used for the evaluation of optical constants of amorphous carbon from laboratory extinction measurements (Rouleau & Martin 1991, Zubko et al. 1996).

According to Mennella et al. (1998), the far-infrared absorption of amorphous carbon nanoparticles is temperature dependent. While cooling down to 24 K, the absolute β value of their BE and ACAR samples increased from 0.95 and 0.8, respectively, to about 1.2, while the mass absorption coefficient at a wavelength of 1 mm decreased by a factor of 3. Again, this behaviour should depend on the electronic structure of the material.

5. Conclusions and Outlook

The experimental investigation of carbonaceous dust analogs will remain a fascinating field of laboratory astrophysics. We can conclude that we reached a first basic understanding of the relation between the structural and optical properties of carbonaceous solids. This is also partly true for thermal annealing processes, hydrogen exposure, and ultraviolet and ion irradiation. We urge astronomers to use the available data in their dust models and to recognize that the world of solid carbon is more complicated than just the crystalline allotropes bulk graphite and diamond. The application of bulk optical properties to small particles has to be taken with care. Onion-type nanoparticles with curved graphitic layers are a good candidate for the UV bump. The spectroscopic in-situ analysis of small particles of stardust origin found in meteorites and interplanetary dust grains will be an interesting route to connect laboratory studies with astronomical observations. An open field is to clarify the role of nitrogen for carbonaceous structures.

We achieved less progress in the complicated area of carbon grain formation. The coupling of size-selective and well-defined production processes, mass spectroscopy, and high-resolution electron microscopy at the atomic level together with a comprehensive theoretical treatment are the tools to make progress in this field. Astronomical observations of circumstellar shells with high spatial resolution, demonstrating any change in feature profile, will be extremely helpful to guide the experiments.

Acknowledgments. Research in Laboratory Astrophysics in Jena and Heidelberg is supported by the DFG research group "Laboratory Astrophysics" Chemnitz/Jena and a joint agreement between the University of Jena and the Max Planck Institute for Astronomy in Heidelberg. Our collaborators J. Dorschner, F. Huisken, M. Schnaiter, and I. Llamas contributed with their research and many discussions to this paper. We thank C. Bailer-Jones for critically reading the paper.

References

Allamandola, L.J., Sandford, S.A., Tielens, A.G.G.M., & Herbst, T.M. 1992, ApJ, 399, 134

Andersen, A.C., Sotelo, J.A., Pustovit, V.N., & Niklasson, G.A. 2002, A&A, 386, 296

Banhart, F. 1994, Phil. Mag. Letters, 69, 45

Banhart, F. 1999, Rep. Progress Phys., 62, 1181

Banhart, F., & Ajayan, P.M. 1996, Nature, 382, 433

Bansal, R.C., & Donnet, J.-B. 1993, in Carbon Black, eds. R.C. Bansal, & M.-J. Wang (New York: Marcel Dekker), 67

Beegle, L.W., Wdowiak, T.J., Robinson, M.S., & Cronin, J.R., McGehee, M.D., Clemett, S.J., & Gillette, S. 1997, ApJ, 487, 976

Braatz, A., Banhart, F., Henning, Th., Ott, U. 1999, Meteoritics & Planetary Science, 34, Suppl., A16

Braatz, A., Ott, U., Henning, Th., Jäger, C., Jeschke, G. 2000, Meteoritics & Planetary Science 35, 75

Bruce, C.W., Stromberg, T.F., Gurton, K.P., & Mozer, J.B. 1991, Applied Optics, 30, 1537

Buss, R.H., Snow, T.P., & Lamers, H.J.G.L.M. 1989, ApJ, 347, 977

Cau, P. 2002, A&A, 392, 203

Chang, H.C., Lin, J.C., Wu, J.Y., & Chen, K.H. 1995, J. Chem. Phys., 99, 11081

Chhowalla, M., Wang, H., Sano, N., Teo, K.B.K., Lee, S.B., & Amaratunga, G.A.J. 2003, Phys.Rev.Lett, 90, 155504

Cherchneff, I., Barker, J.R., & Tielens, A.G.G.M. 1993, ApJ, 413, 445

Chiar, J.E., Pendleton, Y.J., Geballe, T.R., Tielens, A.G.G.M. 1998, ApJ, 507, 281

Chiar, J.E., Tielens, A.G.G.M., Whittet, D.C.B., Schutte, W.A., Boogert, A.C.A., Lutz, D., & van Dishoeck, E.F., & Bernstein, M.P. 2000, ApJ, 537, 749

Chiar, J.E., Adamson, A.J., Pendleton, Y.J., Whittet, D.C.B., Caldwell, D.A., & Gibb, E.L. 2002, ApJ, 570, 198

Chin, R.P., Huang, J.Y., Shen, Y.R., Chuang, T.J., Seki, H. 1995, Phys.Rev.B, 52, 5995

Clayton, G.C., Gordon, K.D., Salama, F., Allamandola, L.J., Martin, P.G., Snow, T.P., Whittet, D.C.B., Witt, A.N., & Wolff, M.J. 2003, ApJ, in press

Cronin, J.R., & Chang, S. 1993, in The Chemistry of Lifes Origin, eds. J.M. Greenberg et al. (Dordrecht: Kluwer), 209

Cruikshank, D.P. 1997, in ASP Conf. Ser. Vol. 122, From Stardust to Planetesimals, eds. Y.J. Pendleton, & Tielens, A.G.G.M. (San Francisco: ASP), 315

Curl, R.F. 1993, in The Fullerenes, eds. H.W. Kroto, & D.R.M. Walton (Cambridge: Cambridge University Press), 19

de Heer, W.A., & Ugarte, D. 1993, Chem. Phys. Lett., 207, 480

Donnet, J.-B., Bansal, R.C., & Wang, M.-J. 1993, Carbon Black (New York: Marcel Dekker)

Draine, B.T. 1989, in Interstellar Dust, eds. L.J. Allamandola, & A.G.G.M. Tielens (Dordrecht: Kluwer), 313

Dresselhaus, M.S., Dresselhaus, G., & Eklund, P.C. 1996, Science of Fullerenes and Carbon Nanotubes (London: Academic Press)

Duley, W.W. 1994, ApJ, 430, L133

Duley, W.W., & Williams, D. 1981, MNRAS, 196, 269

Duley, W.W., & Grishko, V.I. 2001, ApJ, 554, L209

Ehrenfreund, P., & Charnley, S.B. 2000, ARA&A, 38, 427

Evans, S. 1994, in Properties and Growth of Diamond, ed. G. Davies (London: INSPEC), 68

Fitzpatrick, E.L. 1999, PASP, 111, 63

Fitzpatrick, E.L., & Massa, D. 1986, ApJ, 307, 286

Fitzpatrick, E.L., & Massa, D. 1988, ApJ, 328, 734

Frenklach, M., & Feigelson, E.D. 1989, ApJ, 341, 372

Frenklach, M., & Wang, H. 1994, in Soot Formation in Combustion, ed. H. Bockhorn (Berlin: Springer), 165

Geballe, T., Noll, H.S., Whittet, D.C.B., Waters, L.B.F.M. 1989, ApJ, 340, L29

Gibb, E.L., & Whittet, D.C.B. 2002, ApJ, 566, 113

Goto, M., Maihara, T., Terada, H., Kaito, C., Kimura, S., & Wada, S. 2000, A&AS, 141, 149

Goto, M., Gaessler, W., Hayano, Y., Iye, M., Kamata, Y., Kanzawa, T., Kobayashi, N., Minowa, Y., Saint-Jacques, D.J., Takami, H., Takato, N., & Terada, H. 2003, ApJ, 589, 419

Grishko, V.I., & Duley, W.W. 2002, ApJ, 568, 448

Guillois, O., Ledoux, G., & Reynaud, C. 1999, ApJ, 521, L133

Haddon, R.C. 1993, in The Fullerenes, eds. H.W. Kroto, & D.R.M. Walton (Cambridge: Cambridge University Press), 53

Harris, P.J.F., Tsang, S.C., Claridge, J.B., & Green, M.L.H. 1994, Chem. Soc. Faraday Trans., 90, 2799

Hecht, J.H., Holm, A.V., Donn, B., Wu, C.C. 1984, ApJ, 280, 228

Heidenreich, R.D., Hess, W.M., & Ban, L.L. 1968, J. Appl. Cryst., 1, 1

Heimann, R.B., Evsyukov, S.E., & Kavan, L. (eds.) 1999, Carbyne and Carbynoid Stuctures, (Dordrecht: Kluwer)

Henning, Th. 1998, Chem. Society Rev. 27, 315

Henning, Th., & Mutschke, H. 2000, in ASP Conf. Ser. Vol. 196, Thermal Emission Spectroscopy and Analysis of Dust, Disks, and Regoliths, eds. M.L. Sitko, A.L. Sprague, & D.K. Lynch (San Francisco: ASP), 253

Henning, Th., & Salama, F. 1998, Science, 282, 2204

Henning, Th., & Schnaiter, M. 1998, in Laboratory Astrophysics and Space Research, eds. P. Ehrenfreund, H. Kochan, C. Krafft, & V. Pirronello (Dordrecht: Kluwer), 249

Hepp, H., Siegmann, K., & Sattler, K. 1995, Chem. Phys. Lett., 233, 16

Herlin, N., Bohn, I., Reynaud, C., Cauchetier, M., Galvez, A., & Rouzaud, J.N. 1998, A&A, 330, 1127

Homann, K.-H. 1998, Angew. Chem., 110, 2572

Iijima, S. 1991, Nature, 354, 56

Jäger, C., Mutschke, H., & Henning, Th. 1998, A&A, 332, 291

Jäger, C., Henning, Th., Schlögl, R., & Spillecke, O. 1999, J. Non-Crystalline Solids, 258, 161

Joblin, C., Léger, & Martin, P. 1992, ApJ, 393, L79

Kasper, M., Siegmann, K., & Sattler, K. 1997, J. Aerosol Sci., 28, 1569

Koike, C., Kimura, S., Kaito, C., Suto, H., Shibai, H., Nagata, T., Tanabe, T., & Saito, Y. 1995, ApJ, 446, 902

Kroto, H.W., & Walton, D.R.M. 1993, in The Fullerenes, eds. H.W. Kroto, & D.R.M. Walton, 103

Kuznetsov, V.L., Chuvilin, A.L., Butenko, Y.V., Malkov, I.Y., & Titov, V.M. 1994, Chem. Phys. Lett., 222, 343

Ledoux, G., Guillois, O., Huisken, F., Kohn, B., Porterat, D., & Reynaud, C. 2001, A&A, 377, 707

Lewis, R.S., Ming, T., Wacker, J.F., Anders, E., Steel, E. 1987, Nature, 326, 160

Li, A., & Greenberg, J.M. 1997, A&A, 322, 566

Lin, J.C., Chen, K.H., Chang, H.C., Tsai, C.S., Lin, C.E., & Wang, J.K. 1996, J. Chem. Phys., 1005, 3975

Lonfat, M., Marsen, B., & Sattler, K. 1999, Chem. Phys. Lett., 313, 539

Lucas, A.A., Henrard, L., & Lambin, Ph. 1994, Phys.Rev.B, 49, 2888

Maksimova, N.I., Roddatis, V.V., Mestl, G., Ledoux, M., Schlögl, R. 2000, Eurasien Chemo-Technological J. 2(3-4), 231

Maksimova, N., Mestl, G., Schlögl, R. 2001, Studies in Surface Science and Catalysis, 133, 383

Markel, V.A., & Shalaev, V.M. 2001, JOSA A, 18, 1112

Markel, V.A., Shalaev, V.M., & George, T.F. 2001, in Optics of Nanostructured Materials, eds. V.A. Markel & T.F. George (New York: Wiley), 355

Mennella, V., Colangeli, L., & Bussoletti, E. 1995, A&A, 295, 165

Mennella, V., Colangeli, L., Bussoletti, E., Monaco, G., Palumbo, P., & Rotundi, A. 1995a, ApJS, 100, 149

Mennella, V., Colangeli, L., Blanco, A., Bussoletti, E., Fonti, S., Palumbo, P., & Mertins, H.C. 1995b, ApJ, 444, 288

Mennella, V., Colangeli, L., Palumbo, P., Rotundi, A., Schutte, W., & Bussoletti, E. 1996, ApJ, 464, L191

Mennella, V., Baratta, G.A., Colangeli, L., Palumbo, P., Rotundi, A., Bussoletti, E., & Strazulla, G., 1997, ApJ, 481, 545

Mennella, V., Brucato, J., Colangeli, L., Palumbo, P., Rotundi, A., & Bussoletti, E. 1998, ApJ, 496, 1058

Mennella, V., Brucato, J.R., Colangeli, L., & Palumbo, P. 1999, ApJ, 524, 71

Mennella, V., Brucato, J.R., Colangeli, L., & Palumbo, P. 2002, ApJ, 569, 531

Mennella, V., Baratta, G.A., Esposito, A., Ferini, G., & Pendleton, Y.J. 2003, ApJ, 587, 727

Michel, B., Henning, Th., Stognienko, R., & Rouleau, F. 1996, ApJ, 468, 834

Michel, B., Henning, Th., Kreibig, U., & Jäger, C. 1999, Carbon, 37, 391

Motta, V., Mediavilla, E., Muñoz, J.A., Falco, E., Kochanek, C.S., Arribas, S., Garcia-Lorenzo, B., Oscoz, A., & Serra-Ricart, M. 2002, ApJ, 574, 719

Mutschke, H., Dorschner, J., Henning, Th., Jäger, C., Ott, U. 1995, ApJ, 454, L157

Obraztsova, E.D., Fujii, M., Hayash, S., Kuznetsov, V.L., Butenko, Yu.V., & Chuvilin, A.L. Carbon, 36, 821

Ogmen, M., & Duley, W.W. 1988, ApJ, 334, L117

Ott, U. 2001, Mem. Soc. Astron. Italiana, 72, 433

Ott, U. 2003, in Astromineralogy, ed. Th. Henning (Berlin: Springer), 236

Papoular, R., Conard, J., Giulinao, M., Kister, J., & Mille, G. 1989, A&A, 217, 204

Papoular, R., Breton, J., Gensterblum, G., Nenner, I., Papoular, R.J., & Pireaux, J.-J. 1993, A&A, 270, L5

Pendleton, Y.J., Allamandola, L.J. 2002, ApJS, 138, 75

Pouch, J.J., & Alterovitz, S.A., eds. 1990, Properties and Characterization of Amorphous Carbon Films (Zürich: Trans Tech Publication)

Quinten, M., Kreibig, U., Henning, Th., Mutschke, H. 2002, Applied Optics, 41, 7102

Ravagnan, L., Siviero, F., Lenardi, C., Piseri, P., Barboroni, E., Milani, P., Casari, C.S., Li Bassi, A., & Bottani, C.E. 2002, Phys.Rev.Lett, 89, 285506

Robertson, J. 1991, Prog. Solid State Chem., 21, 199

Robertson, J., & O'Reilly, E.P. 1987, Phys.Rev.B, 35, 2946

Rouleau, F., & Martin, P.G. 1991, ApJ, 377, 526

Rouleau, F., Henning, Th., & Stognienko, R. 1997, A&A, 322, 633

Rotundi, A., Rietmeijer, F.J.M., Colangeli, L., Mennella, V., Palumbo, P., & Bussoletti, E. 1998, A&A, 329, 1087

Sakata, A., Wada, S., Okutsu, Y., Shintani, H., & Nakada, Y. 1983, Nature, 301, 493

Sakata, A., Wada, S., Tokunaga, A., Narisawa, T., Nakagawa, H., & Ono, H. 1994, ApJ, 430, 311

Schnaiter, M., Mutschke, H., Henning, Th., Lindackers, D., Strecker, M., & Roth, P. 1996, ApJ, 464, L187

Schnaiter, M., Mutschke, H., Dorschner, J., Henning, Th., & Salama, F. 1998, ApJ, 498, 486

Schnaiter, M., Henning, Th., Mutschke, H., Kohn, B., Ehbrecht, M., Huisken, F. 1999, ApJ, 519, 687

Scott, A.D., Duley, W.W., & Jahani, H.R. 1997, ApJ, 490, L175

Seifert, G., Becker, S., & Dietze, H.-J. 1988, Intern. J. Mass Sectro. and Ion Proc., 84, 121

Shenoy, S.S., Whittet, D.C.B., Chiar, J.E., Adamson, A.J., Roberge, W.G., & Hassel, G.E. 2003, ApJ, 591, 962

Sheu, S.-Y., Lee, I.-P., Lee, Y.T., & Chang, H.-C. 2002, ApJ, 581, L55

Smalley, R.E. 1992, Acc. Chem. Res., 25, 98

Stecher, T.P. 1965, ApJ, 142, 1683

Stecher, T., & Donn, B. 1965, ApJ, 142, 1682

Stognienko, R., Henning, Th., & Ossenkopf, V. 1995, A&A, 296, 797

Tománek, D., Zhong, W., & Krastev, E. 1993, Phys.Rev.B, 48, 15461

Tomita, S., Fujii, M., & Hayashi, S. 2002, Phys.Rev.B, 66, 245424

Tomita, S., Fujii, M., Hayashi, S., & Yamamoto, K. 1999, Chem. Phys. Lett., 305, 225

Ugarte, D. 1992, Nature, 359, 707

van Kerckhoven, C., Tielens, A.G.G.M., & Waelkens, C. 2002, A&A, 568, 584

von Helden, G., Hsu, M.-T., Kemper, P.R., & Bowers, M.T. 1991, J. Chemical Physics, 95, 3835

Wada, S., Kaito, C., Kimura, S., Ono, H., & Tokunaga, A.T. 1999, A&A, 345, 259

Weselowski, P., Lyutovich, Y., Banhart, F., Carstanjen, H.D., Kronmüller, H. 1997, Appl. Phys. Lett., 71, 1948

Willner, S.P., Russell, R.W., Puetter, R.C., Soifer, B.T., & Harvey, P.M. 1979, ApJ, 229, L65

Witt, A.N., Gordon, K.D., Furton, D.G. 1998, ApJ, 501, L11

Wright, E. 1988, Nature, 336, 227

Zubko, V.G., Mennella, V., Colangeli, L., & Bussoletti, E. 1996, MNRAS, 282, 1321

Zwanger, M.S., Banhart, F., Seeger, A. 1996, J. Cryst. Growth, 163, 445